Available online at www.sciencedirect.com
SCIENCE DIRECT®
ELSEVIER
Nuclear Instruments and Methods in Physics Research A 539 (2005) 312–320
NUCLEAR INSTRUMENTS & METHODS IN PHYSICS RESEARCH Section A
www.elsevier.com/locate/nima

Kirkpatrick–Baez microfocusing optics for thermal neutrons

Gene E. Ice[a,*], Camden R. Hubbard[a], Bennett C. Larson[a], Judy W. L. Pang[a], John D. Budai[a], Stephen Spooner[a], Sven C. Vogel[b]

[a]*Oak Ridge National Laboratory, Rm B260, P.O. Box 2008, Bldg. 4500S, MS-6118, Oak Ridge, TN 37831-6118, USA*
[b]*Los Alamos National Laboratory, USA*

Received 8 April 2004; received in revised form 19 July 2004
Available online 18 November 2004

Abstract

Kirkpatrick–Baez neutron supermirrors can efficiently focus neutron beams into small areas with a maximum divergence that is limited by the mirror critical angle. The size of the focal spot is primarily determined by geometrical demagnification of the source and by figure errors in the mirror shape. Ray-tracing calculations show that high-performance Kirkpatrick–Baez supermirrors can preserve neutron-source brilliance when focusing down to tens of microns and can focus approximately two orders of magnitude greater power into 100 μm than is practical without focusing. The predicted performance is near the theoretical limit set by the source brilliance. We describe the phase space arguments, ray-tracing calculations and actual performance of an M3 supermirror system designed to produce a focal spot below 100 μm. Although the current design is optimized for neutron polychromatic microdiffraction, the design principles are widely applicable to a range of neutron science.
© 2004 Elsevier B.V. All rights reserved.

Pacs: 29.3.O.Hs; 29.25.DZ; 61.12.−q

Keywords: Neutron focusing; Kirkpatrick–Baez; Supermirrors; Neutron microbeams

1. Introduction

Neutron supermirrors work as a *specularly reflecting* (angle in equals angle out) short-wavelength filter for thermal neutrons; they efficiently reflect neutrons with wavelengths greater than a critical wavelength. Because they have larger scattering angles than alternative wide-bandpass optics, they are attractive for microfocusing neutrons in the Kirkpatrick–Baez geometry. The Kirkpatrick–Baez neutron optics described here are conceptually identical to X-ray Kirkpatrick–Baez (KB) mirror optics that are widely used to focus X-rays at large demagnifications [1–4]. In the KB design, beam divergences in the horizontal- and vertical-beam planes are focused sequentially

*Corresponding author. Tel.: +1 865 574 2744; fax: +1 865 574 7659.
E-mail address: icege@ornl.gov (G.E. Ice).

0168-9002/$ - see front matter © 2004 Elsevier B.V. All rights reserved.
doi:10.1016/j.nima.2004.10.005

by crossed mirrors that each focus in their plane of scatter (Fig. 1). X-ray focal spots below 80 nm have recently been reported [5] and intensity gains of 10^4–10^5 are common [6,7]. With neutron sources, the typically large source size requires an intermediate aperture to create a small focal spot size. The large neutron source size also decreases the fraction of the source that can be focused, although as described below, focusing optics still provide orders of magnitude more flux on small sample volumes than alternative methods when beam defining apertures cannot be placed very near the sample.

Practical neutron and X-ray mirror designs are remarkably alike due to their similar scattering angles. For example, dense total-external-reflection X-ray mirrors have a critical angle of

$$\theta_{\mathrm{c\,X\text{-}ray}}\,(\mathrm{rad}) = 0.065\lambda\,(\mathrm{nm}). \tag{1}$$

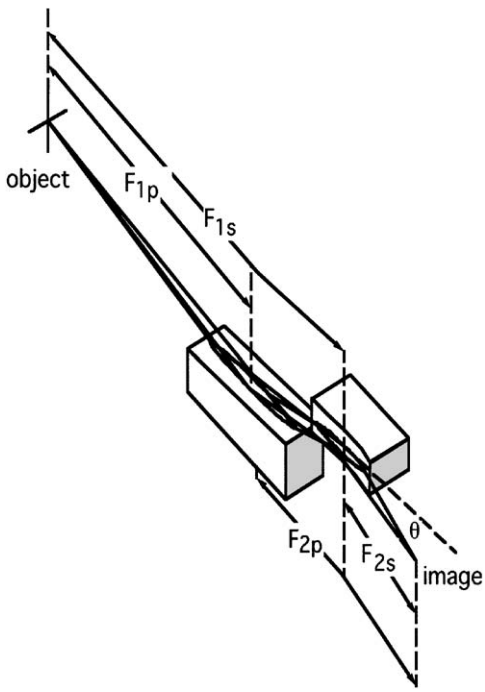

Fig. 1. Kirkpatrick–Baez mirror pair. The object is focused to a real image by sequential focusing in the vertical/beam plane and horizontal/beam plane. The system has asymmetric demagnification but focuses at the same image plane. $F_{1\mathrm{P}}$, $F_{1\mathrm{S}'}$, $F_{2\mathrm{P}}$ and $F_{2\mathrm{S}}$ are the object and image distances for the primary (p) and secondary (s) mirrors.

At angles above this value X-rays with wavelength shorter than λ are inefficiently scattered. Neutron supermirrors have a very similar critical angle given by

$$\theta_{\mathrm{c\,neutron}}\,(\mathrm{rad}) = \frac{M}{56.5}\lambda\,(\mathrm{nm}) \approx 0.064\lambda\,(\mathrm{nm})_{M=3.6}. \tag{2}$$

Here, the M value refers to the ratio of the supermirror critical angle compared to the critical angle of a nickel total-external-reflection neutron mirror. Neutron mirrors with M values between 2 and 3.6 are available and with $M = 3.6$, the neutron critical wavelength is virtually identical to those of X-ray mirrors (Eqs. (1) and (2)). As is clear from Eqs. (1) and (2), both X-ray and neutron mirrors scatter at glancing angles for wavelengths around 0.1 nm.

A consequence of Eq. (2) is that focused neutron supermirrors have a trade-off between collected solid angle, convergence at the sample and the critical wavelength. For our micro-Laue application, a neutron wavelength down to at least 0.08 nm is essential. This dictates a critical angle below ~3 mrad with an M2 mirror and below ~5 mrad for an M3.6 mirror.

The basic equation for mirror focusing in the plane of scatter is

$$R = \frac{2F_1F_2}{(F_1 + F_2)\sin\theta}. \tag{3}$$

Here, F_1 is the object distance, F_2 is the image distance and θ is the nominal mirror glancing angle (Fig. 1). We have studied the design and theoretical performance of a Kirkpatrick–Baez neutron mirror system optimized to produce neutron beams below ~100 μm. This design goal was chosen to increase useable flux for neutron polychromatic (Laue) microdiffraction where good spatial and momentum transfer resolutions are essential and where neutron flux is ultimately limited by the source brilliance. A practical working distance of at least 100 mm from the end of the second mirror was chosen to allow for sample environments, manipulators and detectors. Ray-tracing calculations of the model KB mirror system were found to nearly conserve source brilliance within the image size and focused

divergence; this is *as good as is theoretically possible with linear optics*. The system was also found to outperform more traditional neutron optical systems for small beams. For large beams, the ability to pass larger divergences onto the sample is an advantage of waveguides, polycapillary optics and other approaches.

1.1. The need for focusing

Although guide tubes and collimators work well for large neutron sources and large samples, focusing becomes increasingly important as the neutron probe dimension becomes small. Phase space arguments provide a formal way to compare various methods of achieving small probes and provide a way to understand the relative advantages of different beamline optics. In a phase space diagram [8,9], the beam divergence and position distributions along the beam are represented by contour maps that typically show the e^{-1} intensity contour in either of the two orthogonal axes to the average beam direction (e.g. vertical and horizontal). As illustrated in Fig. 2a, a neutron source is typically large (x dimension) with an almost isotropic divergence (x' dimension representing the momentum perpendicular to the beam axis). An ideal guide limits the beam divergence and beam size but otherwise efficiently transports the phase space from near the source to the end of the tube (Fig. 2b). At the end of the guide tube a slit can be used to further reduce the beam size (Fig. 2c). As the beam propagates away from the slit, the phase space pattern shears, as shown in Fig. 2d. If a sample intercepts the beam at some distance from the last slit, then the flux density on the sample can be estimated from the area of the phase space (in both transverse dimensions) that intercepts the sample, times the source brilliance (neutrons/sec/$\Delta\lambda$/μm^2/mrad^2).

For large samples, a single slit is adequate to define the beam. For small beams, however, two slits are needed because both beam size *and* divergence must be limited unless the distance from the final slit to the sample is negligible. The presence of a wave guide is essential for large beams where large divergences can be used, but is unimportant for small beams. We have modeled the relative performance of a wave guide followed by two-beam defining slits: the first slit is upstream and the second slit is downstream (closest to the sample). Ray tracing finds that for a given root mean square (RMS) probe size *at the sample*, the largest phase space that can be collected onto the sample occurs when the divergence contribution is about twice that of the last slit (Fig. 3). Hence, if the spacing between the last slit and the sample is the same as the spacing between the beam-defining slits, then the first slit should be twice as large as the last slit. Because of the principle of

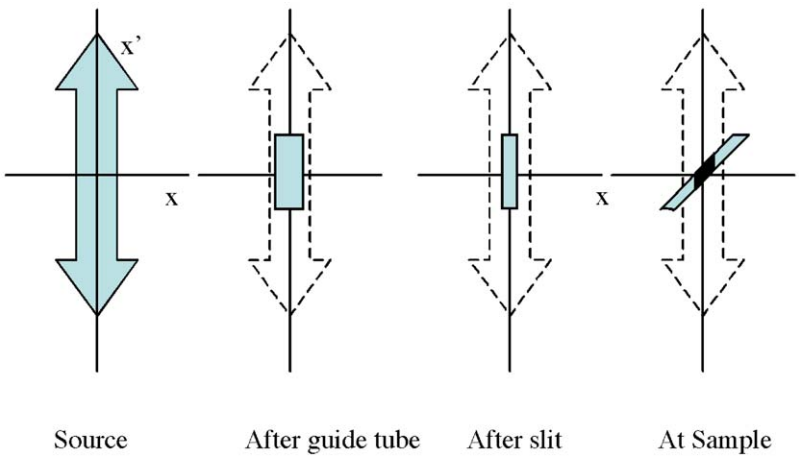

Fig. 2. Phase space diagrams for a neutron beam at the source, after propagation through a guide tube, after an exit slit and at a sample.

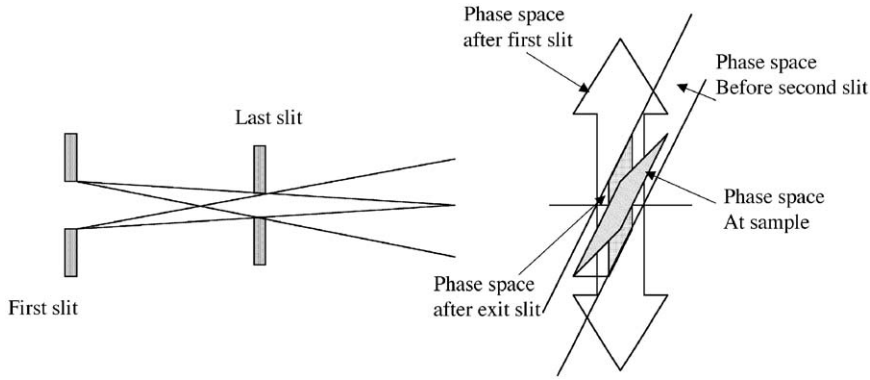

Fig. 3. Geometry for optimized slit-defined beam with the phase space at the sample.

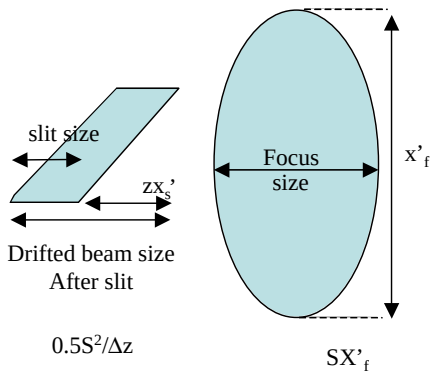

Fig. 4. For a sample size S and a distance ΔZ from the last optical element, the phase space ellipse (in both planes) scales like S for a focusing system and like S^2 for a slit-defined beam (in both axes).

anamorphic drawings, this rule is independent of the distance to the sample or beam size. However, as shown in Fig. 5, the fourth power scaling with beam size of a slit + wave guide optical system becomes quadratic once the divergence passed by the wave guide (or defined by the source size and distance) is reached.

By comparison with a slit and wave guide system, as the required beam size at the sample *decreases* and/or the beam divergence or sample-to-slit distance *increases*, focusing becomes increasingly important. This point is illustrated in Fig. 4, which compares the phase space at the sample with slits and with focusing. With focusing, the beam is condensed to a "waist" at the sample; the phase space ellipse is upright yielding the highest local flux density.

Mirror focused phase space is limited primarily by the length of the mirror and the critical angle; for mirrors, the aperture is roughly the product of the mirror length times its critical angle. With a slit-defined beam, both beam size *and* beam divergence must decrease as beam size at the sample decreases (in both axes). This leads to a fourth power dependence on sample size for the phase space that can be used. With a focusing element there is typically a square dependence on sample size as divergence is independent of spot size. For typical $M\sim3$ supermirrors and assuming 100 mm from the last slit to the sample, the crossover between highest efficiency for slit defined transport and focusing transport is at around 1 mm (Fig. 5). This crossover changes with the distance between the last slit and the sample; for 10 mm slit-to-sample spacing the crossover is at 100 μm and for 0.5 mm slit-to-sample spacing the crossover is at ~4 mm.

1.2. High-performance KB optics compared to alternative focusing methods

It is well known that an ellipse is defined by specular paths between foci with invariant path lengths. In principle, therefore, an elliptical surface specularly condenses rays from one focus to its companion focus with no aberration. Crossed ellipses can focus point-to-point in both dimensions with negligible errors; this is the basis of KB

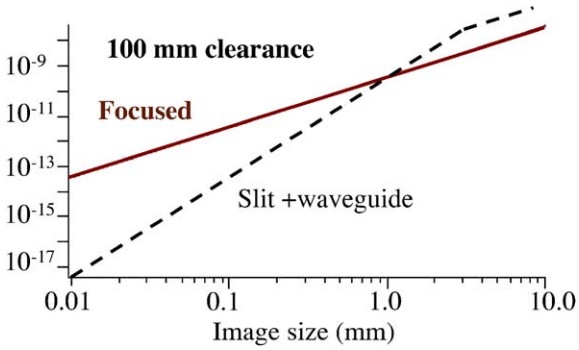

Fig. 5. Ideal fraction of source flux on the sample with KB mirror focusing and a free distance of 0.1 m compared to the maximum fraction of the source flux on the sample with slit-defined beams. The break in slope of the slit-defined beams occurs when the maximum divergence of the source is reached. The maximum beam size that can be passed by KB optics depends on the length of the mirrors. Larger beams can be efficiently collected for KB mirrors with larger focal lengths, but require more stringent figure error tolerance.

mirror pairs. In real applications, however, the source cannot be approximated by a point source and the mirrors are often cylindrical approximations to an ellipse. Focal aberrations introduced by cylindrical approximation to an ellipse are called spherical aberrations. Focal errors introduced by beam size are called coma.

We have performed ray tracing of various KB mirror systems and concluded that cylindrical mirrors introduce only small focusing error for focal spot size in the 100 μm range; coma errors *are very small* for typical geometries we propose. Nearly geometrical demagnifications are predicted under most realistic conditions for elliptical mirrors although other focusing geometries may have problems producing such small beams. For example, ellipsoidal mirrors can have significant aberrations in demagnifying applications. They can be more beneficially used in 1:1 focusing conditions, where they can focus a larger divergence out of the plane of scatter. However, ray tracing shows that even in a 1:1 geometry the aberrations due to the large divergence of the beam are unacceptable and these mirrors cannot compete with KB optics. In addition, toroidal mirrors have such small sagittal radii at these glancing angles, that they are very difficult to manufacture with good surface roughness and figure.

Other focusing designs have been proposed for producing small polychromatic beams [10–16] Short condensing guide tubes [10–13] are similar in performance to slit systems but do not require an upstream guide tube. Polycapillary optics can collect larger divergence onto the source, but are not as efficient as KB mirrors for small beams and small divergences (few milliradian). Refractive optics [15] are typically chromatic. Indeed, unless there is a significantly simpler design or a need to collect a larger convergence onto the sample, there is simply no reason to look beyond the KB mirror system proposed here; within its limited acceptance aperture the KB mirror design adopted for this study is nearly perfect, since it nearly conserves beam brilliance from the source. The RMS divergence and size of a rectangular fraction of the source phase space emittance with dimensions x and x' are $\sigma_x = 0.289x$ and $\sigma_{x'} = 0.289x'$; respectively. The fraction of the total source phase space represented by rectangular patches in both axes is simply $xyx'y'/(\text{sample area})4\pi$. For our design with an $\sim 0.1 \times 0.1\,\text{m}^2$ source and an image with $\sigma_x = \sigma_y = 50\,\mu\text{m}$ and $\sigma_{x'} = \sigma_{y'} = 1.6\,\text{mrad}$, this is about 7.8×10^{-12} of the source phase space; only 1 out of 10^{11} neutrons generated is within the collected phase space. By way of comparison, the fraction of the source collected by a focusing system with the same RMS vertical and horizontal sizes and divergences is 3.8×10^{-12} and the imaged distribution has a peak phase space density that is nearly the same as at the source.

2. Mirror design and calibration

Real mirrors have errors in figure, surface roughness and other deviations from ideal surfaces. We have designed a pair of mirrors with the ability to adapt to a variety of neutron source and sample distances. The prototype mirrors were designed for proof-of-principle and are therefore more flexible (more complicated) than a dedicated system.

The assembled mirror system is shown in Fig. 8. Compared with the cost of high-performance neutron sources, the cost of the focusing prototype

is very modest: ~$30 K for the bending mechanism, tilt/positioning motors, mounts and mechanical support and ~$30 K for three sets of supermirrors. The primary mirror is ~600 mm long × 100 mm wide × 10 mm thick. The secondary mirror is ~200 mm long × 50 mm wide × 10 mm thick.

Prior to coating, the mirror figure was tested at the Advanced Photon Source metrology laboratory using a long-trace profiler. The measured figure errors were relatively large for superpolished mirrors (~10 μrad), but were well within the ~35 μrad tolerance required to limit figure error blurring to less than 100 μm. The mirrors were coated with M3 surfaces and the reflectivity was measured as a function of angle and wavelength at the factory. The mirror reflectivities were ~62–70% at $M = 3$.

Both mirrors are bent by a simple leaf spring mechanism pioneered by scientists at the ALS [16] (Fig. 6). In this design, leaf springs are rigidly attached to the mirror ends. The leaf springs are mounted onto a base that can be lengthened under the mirrors. As the base is spread, the leaf springs bend into S shapes that put equal but opposite bending moments on the two ends of the mirrors. The mirror is pushed near the surface to put nearly equal and same sign moments at the two ends. By superposition of these two bending techniques the mirror surface can be bent to a surface that approximates an ellipse.

3. Experiment

The experimental setup is illustrated in Fig. 7. The mirrors were mounted in the hutch of flight path 5 at the Los Alamos Neutron Science Center (Fig. 8). A small adjustable BN aperture was placed at the beam entrance to the hutch. The slit was set to 3 mm vertically × 1 mm horizontally. The primary (horizontally deflecting mirror) had an object distance of about 4.0 m with an image distance of 0.65 m; magnification = 0.16. The second (vertically deflecting) mirror had an object distance of 4.4 m with an image distance of 0.25 m; magnification = 0.057. A movable BN knife edge was mounted at the focal plane and could be arranged to measure either the horizontal or vertical focused beam size.

Because no real-time neutron area detector was available, the mirror angles and curvatures were optimized with a laser that was aligned along the nominal neutron beam axis. Measurements of the beam size were then made at several mirror angles to seek the optimum focusing conditions. This method was fairly tedious and because of limited time it is very likely that the focal conditions were not optimized.

The beam was detected with a scintillation counter and binned according to the wavelength based on the time of arrival. One real annoyance was the large background in the detector. As shown in Fig. 9, even when the doubly focused beam was fully blocked by the BN knife edge, a large background was observed in the detector. This background is believed to arise from high-energy neutrons and gamma rays that are emitted with an exponential temporal decay after the proton beam strikes the target. Because only a small fraction of the thermal beam passed the $1 \times 3\,\mathrm{mm}^2$ object slit, the background from the high-energy neutrons and gamma rays appeared unusually large for these experiments. This beam

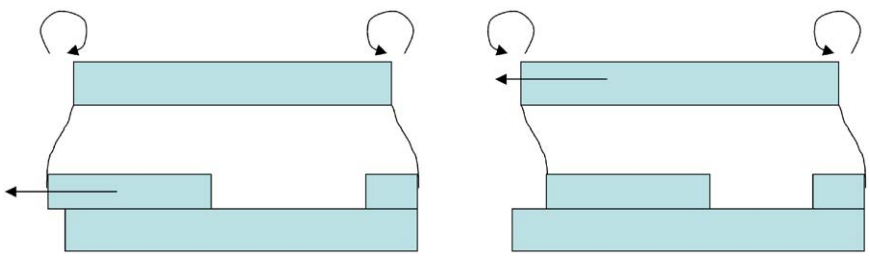

Fig. 6. Bending principle for providing adjustable bending moments on each end of the rectangular mirrors. Spreading the base places moments of equal magnitude but opposite sign on the two ends of the mirrors. Pushing the mirrors places equal moments on the ends of the mirrors.

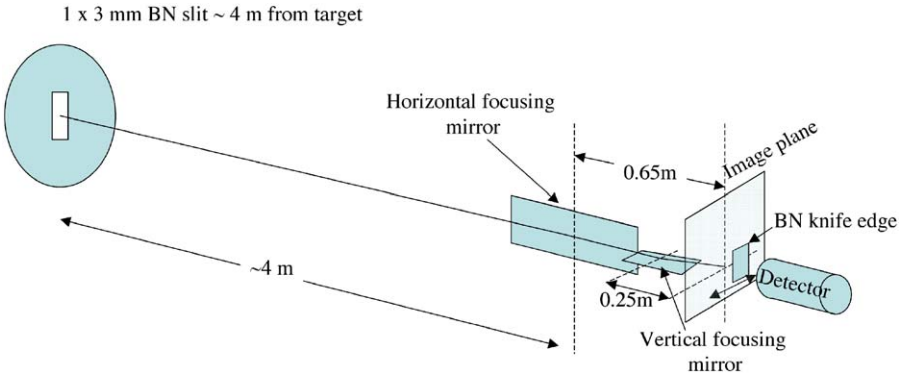

Fig. 7. Experimental setup with dimensions.

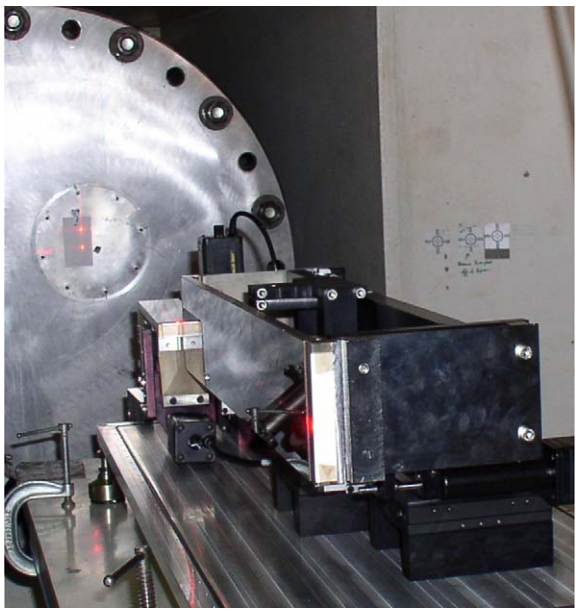

Fig. 8. Crossed mirrors shown on flight path 5 at LANSCE. The mirrors are shown during calibration measurements made with a laser. The mirrors were aligned to a laser that was directed along the centerline of flight path 5.

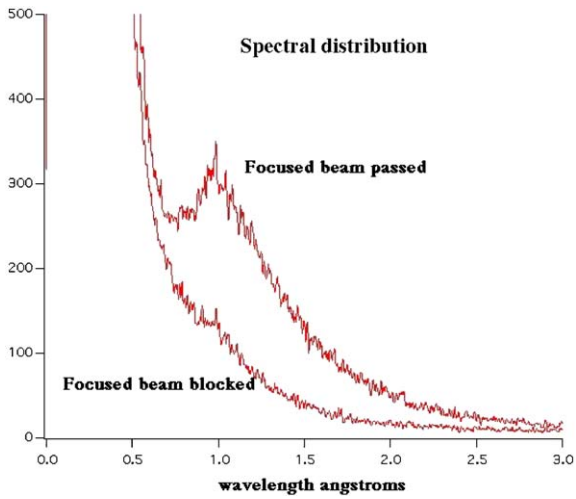

Fig. 9. Neutron spectra detected with the focused beam either fully blocked (bottom) or fully open (top).

can, in principle, be removed by careful shielding and by deflecting the thermal beam out of the main beam path by an upstream mirror. Attempts to reduce this background by the placement of borated polyethylene, forming a long slit in front of the BN slit, helped, but much more could be done on an instrument optimized for microbeam applications. Because the background counts represented a substantial fraction of the focused thermal neutron flux, the background was removed by fitting the spectral distribution at around 0.3 Å and subtracting the scaled fully blocked beam spectra from the spectra at other knife-edge settings. Each spectrum was collected for 15 min and the spectral distributions were averaged over 20 channels to improve the statistical uncertainty. The observed fluctuations are outside the statistical uncertainty and are believed to result from uncorrected changes in the integrated current during the measurements.

4. Results

Knife-edge scans through the doubly focused beam were measured at wavelengths from 0.8 to 1.5 Å were fit with a simple arc tangent function. This assumes a Lorentzian image shape. The vertical and horizontal scans and fits are shown in Fig. 10. For all wavelengths the inflection point of the arc tangent fits agreed within a few microns. Similarly the FWHM were very similar although noise introduced by the background was much larger at 0.08 nm than at 0.15 nm. In addition, steps of 100 μm were used for the vertical scan, which made the uncertainty in the spot size much higher for this direction than for the horizontal scan, where a step size of 50 μm was used near the focus. The vertical spot size had a fit FWHM of 105 ± 33 μm; (145 μm at 0.1 nm, 108 μm at 0.12 nm and 64 μm at 0.15 nm). The measured horizontal spot size was 185 ± 2 μm (185 μm at 0.1 nm, 186 μm at 0.12 nm and 184 μm at 0.15 nm). The theoretical FWHM spot sizes predicted by ray tracing for the conditions of the experiment are $122 \times 152\,\mu m^2$. We note that, due to time constraints, only a single iteration in the mirror angle was attempted for the horizontal focusing. With this iteration the focal spot improved from ~400 μm FWHM to the measured 185 μm FWHM.

The gain of the current system can be estimated from the efficiency of the mirrors, the spot size achieved and the theoretical performance of an ideal KB mirror system compared with an ideal collimator. For a collimator-based system with the same drift distance between the last optical element (150 mm) the ideal gain for $m = 3$ super-mirrors is about 90. Because of the reflectivity of the mirrors and the slightly larger focal spot size than the theoretical, the actual gain achieved is around 37. To achieve similar performance the last slit of a collimator-based system would need to be no farther than 20 mm from the sample.

5. Conclusion

The mirror system illustrated in this paper is only a first step toward the development of intense neutron microbeams. More intense beams can be produced with more aggressive mirror systems that condense somewhat larger divergences onto the sample and therefore have large effective apertures. Such systems are appropriate for low-resolution diffraction experiments, spectroscopy measurements or for experiments with lower momentum transfer needs; longer wavelengths allow for larger divergences. By using KB mirrors

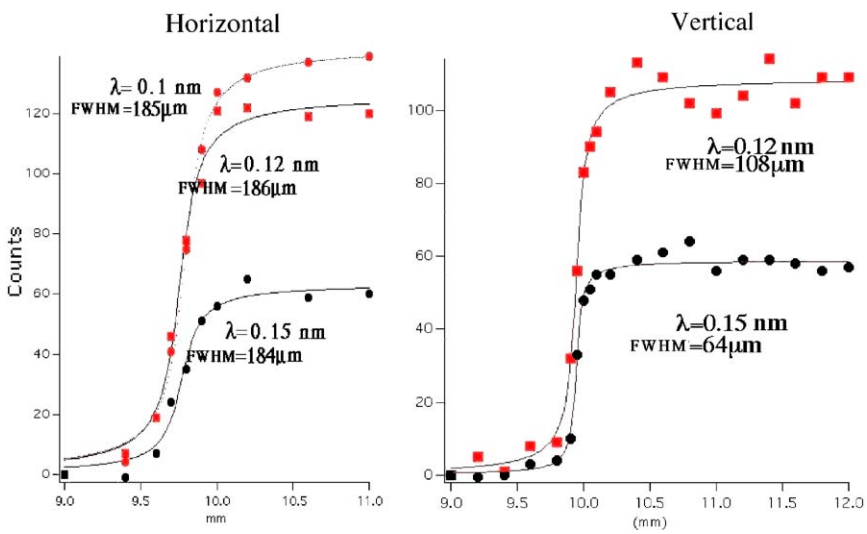

Fig. 10. Fits to the knife-edge scans in the vertical and horizontal directions. The inflection points of all energies are within a few microns of each other both in the horizontal and vertical directions.

that are nested next to each other, the phase space that can be collected can be increased by approximately a factor of two. In addition, by using graded multilayer mirrors with a more limited bandpass, the optical aperture can be significantly enlarged. The choice between focusing optics and wave guides depends on the required probe size, the distance from the last optical element to the sample and the M of the focusing mirror. The figure of merit, FOM, that distinguishes when it is best to use apertures and wave guides and when it is best to use focusing optics is ratio of the sample size, S, to the distance to the last optical element, D; $\mathrm{FOM} = S/D$. For $M = 3$ supermirrors and $\lambda = 1\,\text{Å}$, beamline designers should consider focusing optics when $\mathrm{FOM} < 0.01$.

Acknowledgements

We wish to thank Alastair MacDowell of the Advanced Light Source for the spreadsheet used to calculate the optimum shim thicknesses for the mirrors and Lassen Assoufid for measurement of the mirror figure errors prior to coating. We also wish to thank Cathy Daughtery, Brande Flaitz, Pamela Goidell, Jared Rastoka and Sheila Stevenson for pre-calibrating the mirror curvatures and determining the bending parameters. The research was sponsored by the Laboratory of Directed Research and Development Program of Oak Ridge National Laboratory (ORNL), managed by UT-Battelle, LLC for the US Department of Energy under Contract No. DE-AC05-00OR22725. The work was performed at the Los Alamos Neutron Science Center at Los Alamos National Laboratory. LANSCE is funded by the US Department of Energy under contract W-7405-ENG-36.

The submitted manuscript has been authored by a contractor of the US Government under contract No. DE-AC05-00OR22725. Accordingly, the US Government retains a nonexclusive, royalty-free license to publish or reproduce the published form of this.

References

[1] G.E. Ice, J.S. Chung, J.Z. Tischler, A. Lunt, L. Assoufid, Rev. Sci. Instr. 71 (2000) 2635.
[2] J.H. Underwood, A.C. Thompson, J.B. Kortright, K.C. Chapman, D. Lunt, Rev. Sci. Instr. Abstract 67 (1996) 3359.
[3] P. Kirkpatrick, V. Baez, J. Opt. Soc. Am. 38 (1948) 766.
[4] K. Yamauchi, K. Yamamura, H. Mimura, Y. Sano, A. Saito, A. Souvorov, M. Yabashi, K. Tamasaku, T. Ishikawa, Y. Mori, J. Synchrotron Radiat. 9 (2002) 313.
[5] O. Hignette, P. Cloetens, W.K. Lee, W. Ludwig, G. Rostaing, J. Phys. IV 104 (2003) 231.
[6] P.J. Eng, M. Newville, M.L. Rivers, S. Sutton, SPIE 3449 (1998) 145.
[7] H.A. Padmore, M.R. Howells, S. Irick, T. Renner, R. Sandler, Y.-M. Koo, SPIE 2856 (1996) 145.
[8] T. Matsushita, U. Kaminaga, J. Appl. Crystallogr. 13 (1980) 464 and 472.
[9] G.E. Ice, X-ray Spectrom. 26 (1997) 315.
[10] I.N. Goncharenko, I. Mirebeau, P. Molina, P. Boni, Physica B 234–236 (1997) 1047.
[11] I.N. Goncharenk, I. Mirebeau, A. Ochiai, Hyperfine Interactions 128 (2000) 225.
[12] I.N. Goncharenk, I. Mirebeau, J.-M. Mignot, A. Goukasov, Neutron News 14 (2003) 21.
[13] M.A. Kumakov, V.A. Sharo, Nature 357 (1992) 390.
[14] H. Chen, Nature 357 (1992) 391.
[15] M.R. Eskildsen, P.L. Gammel, E.D. Isaacs, C. Detlefs, K. Mortensen, D.J. Bishop, Nature 391 (1998) 563.
[16] M.R. Howells, D. Cambie, R.M. Duarte, S. Irick, A. MacDowell, H.A. Padmore, T. Renner, S. Rah, R. Sandler, Opt. Eng. 39 (2000) 2748.